EEET ECOLOGICAL ENGINEERING & ENVIRONMENTAL TECHNOLOGY

Ecological Engineering & Environmental Technology, 2026, 27(8), 458–475
https://doi.org/10.12912/27197050/225376
ISSN 2719–7050, License CC-BY 4.0

Received: 2026.06.24
Accepted: 2026.07.10
Published: 2026.08.01

Valorization of iron-rich copper waste mine tailings from Guelb Moghrein (Mauritania) via geopolymerization: Reaction mechanisms, microstructure and mechanical performance

Chikh Sidi EL Mokhtar Mohamed Lefdhil[1*], Ahmed Hamoud[1], Oumayma Nassiri[2], Ahmedou Mahfoudh[1], Aminetou Kebd[1], Khaled Cheikh Nebaghe[1], Ahmed Ould Brahim[3], David Martínez Poyatos[4]

[1] Department of Geology, Research Unit Geosciences, University of Nouakchott Al-Aasriya, Mauritania
[2] Cadi Ayyad University, École Normale Supérieure de Marrakech, Interdisciplinary Research Laboratory in Bioresources, Environment, and Materials, BP 2400 Hay Hassani Route d'Essaouira 40000, Marrakech, Morocco
[3] Department of Chemistry, University of Nouakchott Al-Aasriya, Nouakchott, Mauritania
[4] Departamento de Geodinámica, Universidad de Granada, Granada, Spain
* Corresponding author's e-mail: chikhsidielmoctar@gmail.com

ABSTRACT

The increasing production of waste mine tailings constitutes a major environmental challenge, requiring the development of sustainable valorization strategies. This study assesses the feasibility of synthesizing geopolymers from Mauritanian iron-rich copper mine tailings, aiming to elucidate the influence of iron-rich phases on geopolymer formation and performance. The tailings samples were mixed with metakaolin (MK) at different mass ratios (100:0, 50:50, and 0:100). The precursors were ground, and the MK was calcined at 750 °C to ensure its amorphization. The geopolymers were activated using a 12M KOH alkaline solution (Si/Al = 1.30). The resulting materials achieved a uniaxial compressive strength of up to 8.5 MPa, demonstrating geopolymerization potential for new construction materials. Microstructural and mineralogical analyses (XRD, FTIR, SEM-EDS) supported the formation of a K-A-S-H-type geopolymeric matrix and suggested the possible contribution of iron-bearing phases to the aluminosilicate network development. Optical microscopy observations on polished thin-sections confirmed these results, highlighting the transformation of the mineral phases of the original waste mine tailings into an amorphous geopolymer matrix, thus confirming the successful alkali activation of the precursors. The research line provides with a promising pathway for sustainable mining waste management via producing new, ecofriendly, construction materials in a modern circular economy system.

Keywords: iron-rich waste mine tailings, metakaolin geopolymer, alkaline activation, Fe-bearing phases, mineralogy, microstructure, compressive strength, waste valorization.

INTRODUCTION

Current industrial and urban development is facing a major environmental challenge. On one hand, the global demand for construction materials, particularly aggregates and sand, is depleting natural resources, while cement production remains one of the primary sources of CO_2 emissions [1, 2]. On the other hand, the extractive industry generates large volumes of mining waste, responsible for severe pollution such as acid mine drainage and soil contamination, due to their hazardous chemical composition [3–7]. Faced with this dual observation, the search for alternative construction materials, such as geopolymers, emerges as a promising solution, particularly due to their low energy consumption [8, 9]. Their production process, carried out at low temperatures, results in significantly lower carbon dioxide (CO_2) emissions compared to conventional Portland cement. Moreover, geopolymers exhibit superior performance, including enhanced mechanical strength and durability, as

well as an exceptional ability to encapsulate heavy metals [7, 10]. Geopolymerization is based on the reaction between an aluminosilicate precursor and an alkaline solution (typically sodium hydroxide (NaOH) or potassium hydroxide (KOH), often combined with an alkaline silicate). The rigid three-dimensional network formed through this process is capable of chemically binding toxic elements, thereby drastically limiting their leaching and migration into the environment [11, 12].

The direct use of waste mine tailings as precursors in geopolymerization faces a major obstacle, their low chemical reactivity. Rich in silica (SiO_2) and iron or poor in alumina (Al_2O_3), these residues create an unfavorable Si/Al ratio that slows the reaction, and a high Fe_2O_3 content ($Fe_2O_3/Al_2O_3 > 0.37$) that reduces the compressive strength, especially since iron can substitute for only about 25% of aluminum atoms in the geopolymer matrix [8, 13–16]. To overcome these limitations, metakaolin (MK) is commonly introduced as a highly reactive aluminosilicate precursor [17]. Its amorphous structure and high Al_2O_3 content enable the adjustment of the Si/Al ratio and promote the dissolution - polycondensation reactions, thereby enhancing geopolymerization kinetics and gel formation [17–19].

Despite growing research on waste mine tailings-based geopolymers, the reactivity of Fe-rich copper tailings remains limited and the optimal balance between waste incorporation and mechanical performance is still unclear, particularly for KOH-activated systems and moderate curing regimes. Furthermore, Mauritanian mining waste has never been investigated as a geopolymer precursor, representing an unexplored opportunity for sustainable mining waste management.

The scientific novelty of this study lies in the investigation of a highly challenging iron-rich copper tailing derived from the Guelb Moghrein Fe-Cu-Au structurally modified iron-copper-gold (IOCG) type deposit, characterized by an exceptionally high Fe_2O_3 content and complex mineralogical assemblage. Unlike conventional geopolymer studies focusing mainly on reactive aluminosilicate precursors, this work provides new insights into the role of iron-bearing phases during alkaline activation by establishing relationships between Fe-rich mineralogy, geopolymer gel development, microstructural evolution, and mechanical performance. In addition, this study evaluates the maximum incorporation level of this mining residue while maintaining acceptable mechanical properties through metakaolin-assisted geopolymerization.

Accordingly, this study aims to (i) optimize the tailings-to-metakaolin ratio to maximize waste incorporation while maintaining mechanical performance, (ii) evaluate the effect of curing time on compressive strength, and (iii) correlate phase evolution, the contribution of Fe-bearing phases, and microstructural development with mechanical behavior.

MATERIALS AND METHODS

This section describes the raw materials and the experimental framework used to evaluate the feasibility of geopolymerizing iron-rich copper waste mine tailings from Guelb Moghrein Cu-Au mine (Mauritania). An integrated analytical approach was implemented to assess their reactivity, mineralogical evolution, and the resulting microstructural and mechanical performance of the synthesized geopolymeric materials.

Raw materials

The Guelb Moghrein Cu-Au deposit is located in the upper succession of the volcanosedimentary Oumachoueima Group. This group forms part of the fold & thrust, low-grade metamorphosed, Mauritanian Belt that thrust to the East on the western edge of the Archean Amsaga continental basement (West African craton) and its unconformable Paleozoic Taoudeni sedimentary cover (Figure 1). Unless unfossiliferous, the upper formations of the Oumachoueima Group have been recently attributed to the Ediacaran (late Neoproterozoic) based on U/Pb detrital zircon dating [20]. The upper Oumachoueima Group includes metamorphosed carbonate banded iron formations (BIF). The BIF that hosts the ore deposit consists of pistomesite-magnetite metacarbonates, as well as Fe-Mg clinoamphibole and chlorite schists, which also contain magnetite, apatite, calcite, quartz, monazite, and allanite [21–23]. The hydrothermal mineralization is classified as an IOCG-type deposit, hosted within a coarse-grained ferromagnesian carbonate unit (FMC). The main sulfide minerals are chalcopyrite, pyrrhotite, and magnetite [22, 24, 25]. Open-pit mining commenced in April 2006, followed by the initiation of sulfide ore processing in July 2006 to produce a copper-gold concentrate [23]. In 2015, the plant produced

17,000 tons of concentrate per month with a grade of 22.5% Cu, along with gold as a by-product. The total annual production reached 45,001 tons of copper and 47,322 ounces of gold, from a total extracted volume of 27.5 Mt (including 3.8 Mt of ore and 23.7 Mt of waste rock) [26, 27].The waste mine tailings generated from ore processing are subsequently deposited in nearby tailings storage facilities (TSF): TSF1 (2007, 53 ha), TSF2 (2009, 162 ha), and TSF3 (2015) (Figure 1).

The kaolin used as a precursor raw material in this study was supplied by SANIMED, a Tunisian ceramic manufacturing company

Sampling and preparation procedures of raw materials

Sampling was carried out at various locations within the TSF1 in accordance with UNE-EN 932-1 [29]. A total of 10 samples were collected according to a predefined plan and site accessibility. For each sample, the shallowest surface deposit layer was removed, and material from the top 0–7 cm was collected using a hand shovel. Samples were placed in labeled polyethylene bags and subsequently mixed and homogenized using the quartering method to obtain a representative composite sample, referred to as TSFr. All sample portions were preconditioned to achieve a stable and reproducible physicochemical state prior to analysis. Subsequently, they were homogenized and reduced to representative subsamples to minimize intrinsic heterogeneity following UNE-EN 932-2 [30]. They were then finely ground (<125 µm) to ensure sufficient compositional uniformity and to enhance the reliability and precision of chemical and mineralogical characterizations.

Characterization of raw materials

Several analytical and microscopy techniques were employed to determine the physical, chemical, and mineralogical characteristics of the waste mine tailing. Polarized-light optical microscopy images (Dept. Mineralogy and Petrology, UGR) were adquired in transmision- and reflection-light modes on ultrapolished thin-sections (~30 µm-thick). The raw materials were analyzed by X-ray diffraction (XRD) (Dept. Mineralogy and Petrology, UGR). Whole-sample fractions were prepared as disoriented powders after milling in an agate mortar. A PANalytical X'Pert Pro diffractometer (MalvernPanalytical, Malvern, UK) was employed to study whole fractions, using Cu Kα radiation, 45 kV, and 40 mA. The diffractometer is equipped with an X'Celerator solid-state linear detector, which produced an overall counting time of 10 s/step, with step increments of 0.008° 2θ. XRD diagrams were interpreted with HighScore and free software. Fourier-transform infrared

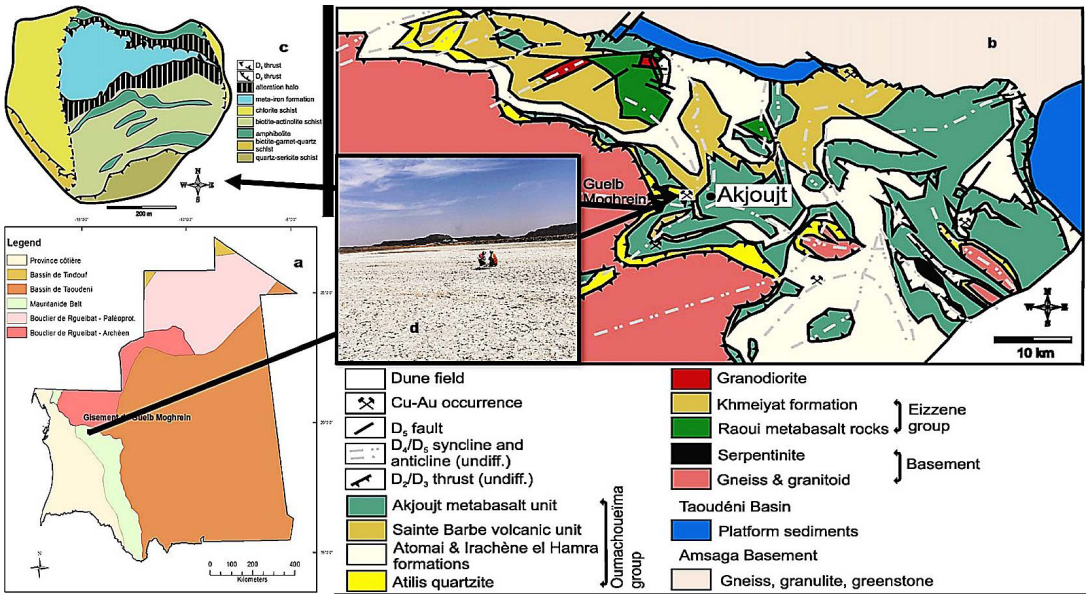

Figure 1. Location and geological context of the Guelb Moghrein Cu-Au deposit (Akjoujt): (a) location in Mauritania; (b) regional geological map (adapted from [25] after [21]; (c) detailed geological map of the Guelb Moghrein mine [28] ; d) field view of the sampling waste mine tailing storage site TSF1

spectroscopy (FTIR) was performed using a FTIR spectra (4000–400 cm^{-1}, resolution 0.25 cm^{-1}) on raw solid samples. FTIR analyses were acquired with a JASCO 6200 spectrometer with software SPECTRA MANAGER v2 (Scientific Instrumentation Center, UGR) equipped with an ATR accessory, using transmission mode, to identify the main functional groups and complement XRD analysis.

The microstructure (on raw surfaces and ultra-polished thin-sections) and elemental chemistry (in-situ microanalysis and compositional maps) of the raw material samples were characterized by scanning electron microscopy (SEM) (Scientific Instrumentation Center, UGR). Microstructural characterization was performed using a field-emission environmental scanning electron microscope (FEG-ESEM), FEI Quanta/QuEMSCAN 650F, equipped with a Schottky field emission gun (FEG), a beam deceleration system, and multiple electron detectors for high-resolution imaging and compositional analysis. Secondary electron (SE) images were acquired at an accelerating voltage of 5 kV using the ETD detector under high-vacuum conditions. The low accelerating voltage was selected to minimize charging effects and to improve the observation of fine surface morphological features. The microscope operating conditions were optimized to obtain high-resolution, low-noise images. Elemental microanalysis was conducted at 20 kV using a dual energy-dispersive X-ray spectroscopy (EDS) system from Bruker equipped with two XFlash 6/30 silicon drift detectors (SDD). Each detector had an active area of 30 mm^2 and an energy resolution better than 129 eV at Mn Kα (100,000 cps). The dual-detector configuration improved X-ray collection efficiency and analytical sensitivity, enabling reliable elemental characterization, including the detection of light elements from boron onward through the use of ultralight detector windows. Compositional contrast imaging was obtained using the CBS solid-state backscattered electron (BSE) detector. This detector is segmented into concentric sections that allow angular discrimination of backscattered electrons, providing enhanced compositional contrast based on differences in atomic number between phases. These approaches provided detailed insights into particle morphology, aggregation features, and microscale mineral heterogeneities.

Whole-sample, major-elements (oxide-) concentrations were determined by X-ray fluorescence (XRF) using a ZETIUM spectrometer (Research, Technology and Innovation Center, Univ. Seville, Spain). Analyses were performed with the WROXI PRO method. Whole-sample powders were fused with lithium tetraborate prior to measurement. Analytical precision was typically better than ±1.5% for analyte concentrations around 10 wt.%. XRF quantifies the volatile content of the samples by means of loss on ignition (LOI). Humidity content was also determined by oven-drying at 105 °C to quantify the water present. Calcium carbonate content (% $CaCO_3$) was measured using a Bernard calcimeter, and pH measurements provided additional information on the chemical characteristics of the waste mine tailings. To ensure data reliability, all analyses were performed in triplicate.

Geopolymer sample preparation

The mining tailings (TSFr) were oven-dried at 105 °C for 24 h until constant mass, subsequently ground, and sieved to obtain a particle size fraction below 125 μm (Figure 2). The metakaolin (MK) used as a reactive aluminosilicate precursor was obtained by calcination of kaolin at 750 °C for 5 h to ensure complete dehydroxylation and the formation of a highly reactive amorphous phase. The alkaline activator consisted of a 12 M KOH solution prepared 24 h before use using analytical-grade potassium hydroxide pellets and distilled water to ensure stabilization of the solution (Figure 2). The geopolymer formulations were prepared by replacing MK with different proportions of TSFr while maintaining constant alkaline activation conditions. The liquid-to-solid (L/S) ratio, defined as the mass ratio between the alkaline activator solution and the total solid precursors, was fixed at 0.8 for all mixtures to maintain comparable workability and ensure consistent activation conditions. The solid precursors were first homogenized by mechanical mixing, followed by gradual addition of the alkaline activator. Mixing was continued for 15 min to obtain a homogeneous geopolymer paste with uniform distribution of the activating solution.

The fresh geopolymer pastes were cast into alkali-resistant cylindrical molds with a diameter of 22 mm and a height of 44 mm (L/D = 2). The specimens were compacted to minimize entrapped air and demolded after 24 h. Curing was performed at a controlled temperature of 60 °C for 7, 14, and 21 days to evaluate the evolution of geopolymer structure and mechanical performance under accelerated curing conditions,

Figure 2. Flowchart of geopolymer preparation: (1) raw materials; (2) MK calcination at 750 °C for 5 h; (3–4) grinding; (5) sieved raw materials; (6) KOH solution preparation; (7) mixing; (8) curing. Lower images illustrate examples of synthesized geopolymer cylinders

following procedures commonly reported for alkali-activated materials [26–31]. Prior to mechanical testing, all specimens were conditioned at room temperature for 24 h to minimize variations related to temperature and moisture content.

All geopolymer formulations were prepared in triplicate to ensure experimental reproducibility. The compressive strength results are reported as the average value ± standard deviation, and error bars were added to represent experimental variability (Table 1).

Geopolymer characterization and testing

The synthesized geopolymers were characterized in terms of their chemical, mineralogical, microstructural, and mechanical properties. The uniaxial unconfined compressive strength (UCS) was determined on cylindrical specimens following the general recommendations of ASTM C39/C39M for compressive testing of cylindrical materials. The tests were performed using a LLOYD LR50K universal testing machine (National School of Engineers of Sfax, Tunisia) controlled by NEXYGEN Plus software, under a constant displacement rate of 2 mm/min until failure.

For each formulation and curing age, three independent specimens were tested, and the results are reported as the mean compressive strength value ± standard deviation. The fracture patterns and crack development after failure were examined to establish relationships between mechanical behavior and microstructural characteristics.

Microstructural, chemical, and mineralogical investigations were performed using optical microscopy, EDS-SEM, X-ray diffraction (XRD), and Fourier-transform infrared spectroscopy (FTIR). These complementary techniques were used to identify phase assemblages, characterize reaction products, and evaluate the evolution of the geopolymeric matrix during alkaline activation.

RESULTS AND DISCUSSION

Characterization of raw materials

Physicochemistry of raw materials

The bulk chemical composition of the TSFr waste mine tailing and MK metakaolinite precursors was determined by X-ray fluorescence (XRF), and the results are summarized in Table 2. The TSFr sample exhibits high concentrations of

Table 1. Raw components proportions and curing times (at 60 °C) used for geopolymer synthesis

Sample ID	TSFr (%)	TSFr (g)	MK (%)	MK (g)	KOH (M)	Curing temperature (°C)	Curing time (days)	L/S
GP:D100.12.T21	100	100	0	0	12	60	21	0.8
GP:D50.12.T21	50	50	50	50	12	60	21	0.8
GP:D0.12.T21	0	0	100	100	12	60	21	0.8
GP:D100.12.T14	100	100	0	0	12	60	14	0.8
GP:D50.12.T14	50	50	50	50	12	60	14	0.8
GP:D0.12.T14	0	0	100	100	12	60	14	0.8
GP:D100.12.T7	100	100	0	0	12	60	7	0.8
GP:D50.12.T7	50	50	50	50	12	60	7	0.8
GP:D0.12.T7	0	0	100	100	12	60	7	0.8

some major oxides, particularly Fe_2O_3 (46.6%), reflecting the abundance of iron-bearing minerals in the waste mine tailings, such as magnetite, hematite, chalcopyrite, pyrrhotite, and arsenopyrite (see next sections). In contrast, MK is characterized by high SiO_2 (51.27%) and Al_2O_3 (36.66%) contents, indicating its suitability as an aluminosilicate source for geopolymer synthesis. The TSFr also contains moderate amounts of MgO (12.93%) and minor quantities of CaO, Na_2O, K_2O, P_2O_5, and SO_3, while other trace oxides such as TiO_2, Mn_3O_4, V_2O_5, and HfO_2 are present at very low levels or below the detection limit. Notably, the LOI of TSFr is 26.25%, which represents the combined weight loss of humidity, organic matter, and carbonates during XRF analysis heating. The MK exhibits a lower LOI of 6.58%, consistent with its more thermally stable nature in comparison with TSFr. These compositional differences highlight the complementary nature of TSFr and MK: TSFr provides with an iron-rich matrix, while MK contributes with the aluminosilicate framework necessary for geopolymer formation.

The physico-chemical properties of the TSFr tailings were investigated to assess their suitability as a geopolymer precursor. Key parameters, including calcium carbonate ($CaCO_3$) content, pH, humidity, and organic matter content, were measured, and the results are presented in Table 2. The TSFr sample exhibits a $CaCO_3$ content of 4%, indicating a minor carbonate fraction that may contribute slightly to alkalinity. The pH value of 7.4 confirms that the tailings are near neutral, which is favorable for alkali activation. The humidity is 6%, reflecting the inherent water present in the material, which could influence the early geopolymerization process and it needs to be considered during material processing.

These properties provide essential baseline information for tailoring the geopolymer synthesis parameters, such as water-to-solid ratio, alkali solution concentration, and curing conditions, in order to optimize matrix phase framework development and thus mechanical performance.

FTIR characterization of raw materials

The FTIR spectra of kaolin and metakaolin can be divided into two main regions: 4000–1350 cm^{-1} and 1350–350 cm^{-1} (Figure 3). In the high-wavenumber region, raw kaolin exhibits characteristic bands between 3600 and 3700 cm^{-1}, attributed to O–H stretching vibrations of structural hydroxyl groups (Al–OH). These bands disappear after calcination, indicating the dehydroxylation of kaolinite and its transformation into amorphous metakaolin [31,32]. In the low-wavenumber region, the band observed around 1030–1110 cm^{-1} is assigned to asymmetric Si–O–Si and Si–O–Al stretching vibrations, characteristic of aluminosilicate frameworks. Additional bands located at approximately 570 and 465 cm^{-1} are attributed to bending vibrations of Si–O–Al and Si–O–Si bonds, respectively [33,34]. The weak band near 1600 cm^{-1} corresponds to the bending vibration of adsorbed water molecules. The overall decrease in band intensity after calcination reflects the structural disorder and increased amorphous nature of metakaolin [35].

The FTIR spectrum of TSFr reveals several absorption bands associated with iron-bearing phases and silicate structures (Figure 3). The

Table 2. Chemical and physico-chemical properties of raw materials (N.D. – not detected)

Parameter	TSFr	MK
Major oxides (%)		
SiO_2	6.20	51.27
Al_2O_3	0.84	36.66
Fe_2O_3 (total Fe)	46.56	1.11
MgO	12.93	0.41
CaO	1.85	0.06
Minor oxides (%)		
TiO_2	0.07	0.14
Mn_3O_4	1.04	N.D.
Na_2O	0.42	0.11
K_2O	0.12	3.46
P_2O_5	0.06	0.08
SO_3	3.48	N.D.
V_2O_5	N.D.	N.D.
HfO_2	N.D.	N.D.
Physico-chemical properties		
L.O.I (%)	26.25	6.58
$CaCO_3$ (%)	4	—
pH	7.4	—
Humidity (%)	6	—

bands observed in the range of 460–570 cm^{-1} are attributed to Fe–O vibrations, suggesting the presence of iron oxides such as hematite and magnetite. The broad band around 3400 cm^{-1} and the band near 1620 cm^{-1} are assigned to O–H stretching and H–O–H bending vibrations, respectively, indicating the presence of adsorbed water and hydroxyl groups [33, 34, 36]. A weak band around 3100–3200 cm^{-1} may be associated with hydroxyl groups linked to iron-bearing minerals such as goethite [35, 37]. Overall, these spectral features confirm the presence of aluminosilicate and iron-rich phases in the studied materials, which is consistent with the XRF results and will be further validated by XRD analysis.

Mineralogical characterization (XRD) of raw materials

The XRD analysis of TSFr reveals a mineralogical assemblage dominated by magnetite, siderite, quartz, muscovite, and dolomite, which is consistent with Fe-rich waste mine tailings reported in the literature [31] (Figure 4). Minor arsenide phases such as lollingite and clinosafflorite may also be present. The high abundance of iron-bearing phases is in agreement with the elevated Fe_2O_3 content obtained from XRF analysis and the magnetic susceptibility properties of the waste mine tailings (Figure 5).

The XRD pattern of metakaolin exhibit a broad amorphous halo in the range of 15°–35° (2θ), characteristic of the transformation of crystalline kaolinite into amorphous metakaolinite (Figure 4). The shift in the halo position reflects structural disorder induced by dehydroxylation during calcination at 750 °C. However, residual crystalline phases, mainly quartz, remain, as indicated by the intense peak at approximately 26° (2θ) [32, 33]. Additional reflections observed at ~20°, 24°, 35°, and 42° suggest the persistence of partially transformed aluminosilicate structures. These

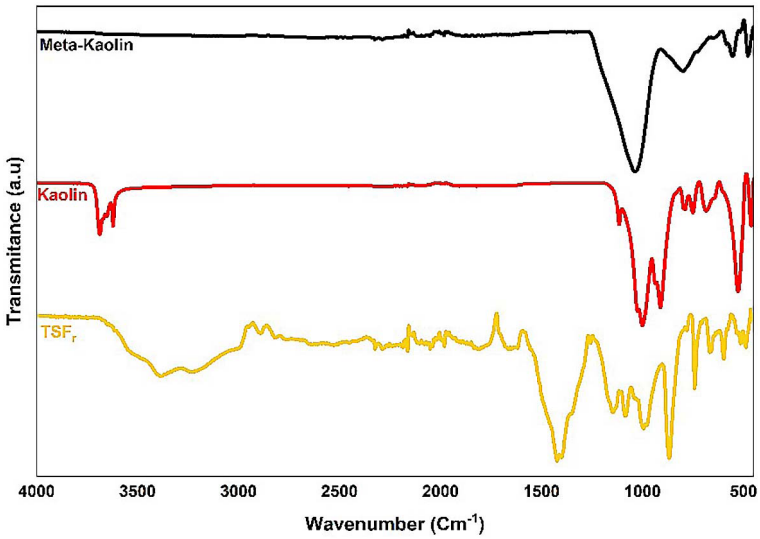

Figure 3. FTIR spectra of raw materials. See text for explanation

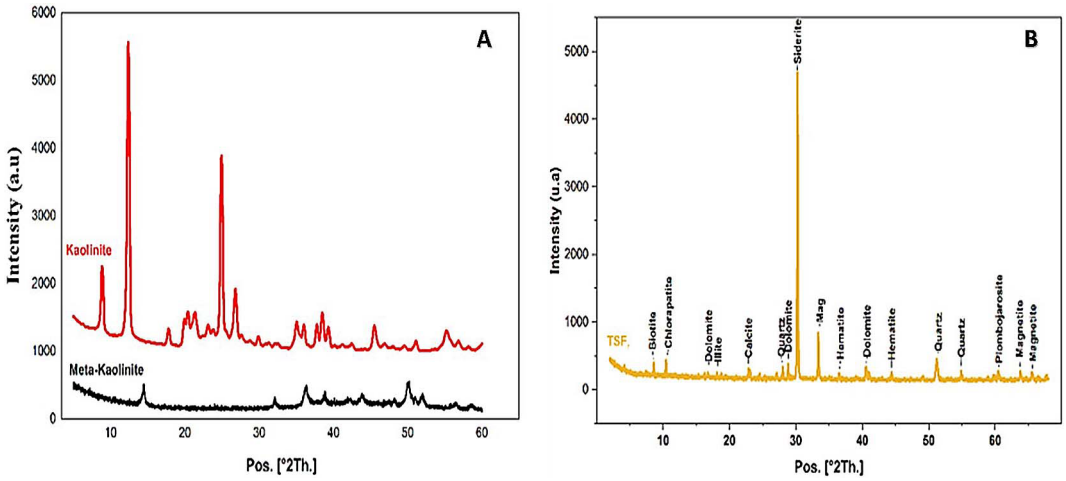

Figure 4. XRD patterns of (a) metakaolin and (b) TSFr

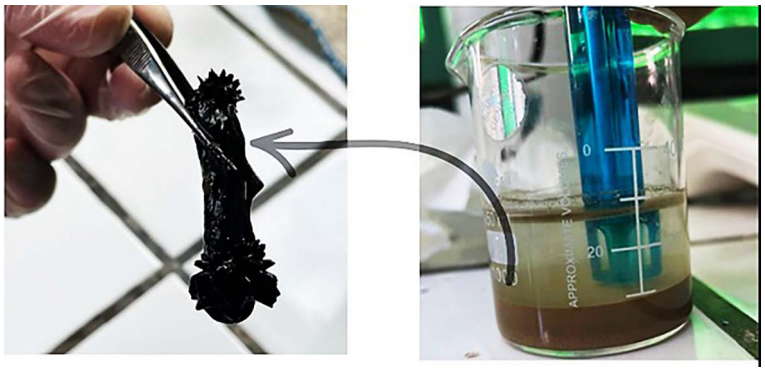

Figure 5. Magnetic behavior of the TSFr

observations are consistent with previous studies. The presence of silica in both TSFr and metakaolin is further supported by FTIR analysis [34–37, 38].

Optical microscopy characterization of waste mine tailing

Ultrapolished thin-sections were made after epoxy resin-induced consolidation of TSFr. Optical microscopy images revealed a non-sorted pool of, ore-inherited, mineral clasts (up to 500 µm-large, ~100–200 µm on average) composed by carbonates, phyllosilicates (muscovite, chlorite, biotite), quartz, Fe-hydroxides, and minor quantities of pyrite, magnetite and K-feldspar (Figure 6). This mineralogical assemblage is consistent with findings from waste mine tailings of similar Fe-rich polymetallic sulfide deposits worldwide, such as those reported by [39] in China and [40] in India. The coexistence of sulfide and Fe-(hydro-) oxidized phases reflects both the original hydrogeochemical conditions of the ore and the subsequent alteration processes during ore processing, waste mine tailings deposition and weathering [41–43]. Such mineral content is commonly observed in Fe-rich mining residues and support the interpretation of XRD and FTIR data.

Characterization of the synthesized geopolymers

FTIR analysis of geopolymers

FTIR spectra of Bir Oumgrein TSF-derived geopolymers reveal both the persistence of precursor mineral phases and the formation of a geopolymeric network. The survival of precursor-related bands after alkaline activation indicates partial dissolution of the tailings (Figure 7). Absorptions in the 800–900 cm^{-1} region are assigned to Si–O stretching of residual silicates. The broad 460–610 cm^{-1} range encompasses silicate framework bending, including contributions from the new geopolymeric gel (Si–O–Al, Si–O–Si). The peak at 639 cm^{-1} is characteristic of residual magnetite, while the shoulder near 1047

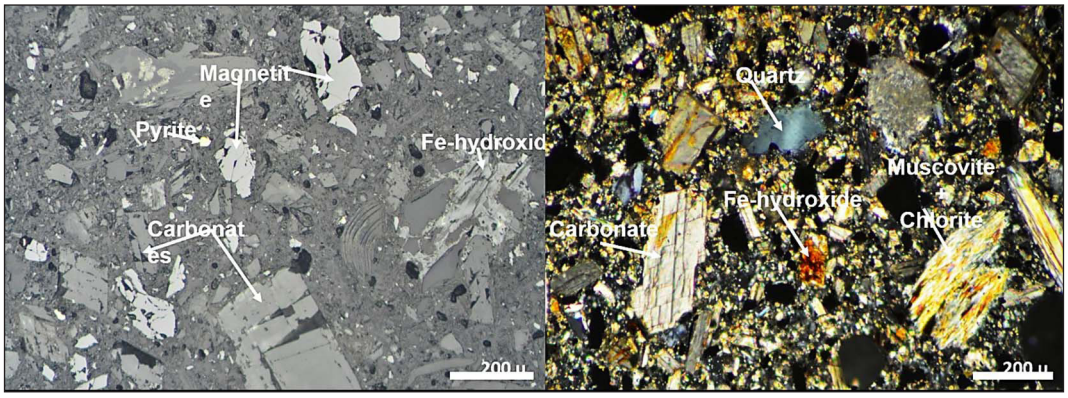

Figure 6. Optical microscopy images of TSFr (consolidated with epoxy resin) ultrapolished thin-section under (a) reflected- and (b) transmitted (cross-polarized)-light

cm^{-1} originates from undissolved aluminosilicates. These features confirm that the Fe-rich phases of the Bir Oumgrein TSF remain largely unreactive under the studied alkaline conditions [40, 44]. Compared with the raw material, a noticeable shift of the main Si–O–T (T = Si or Al) band toward lower wavenumbers, centered around 1000–1010 cm^{-1}, is observed after alkaline activation. [45, 46] This shift reflects the partial dissolution of the original aluminosilicate phases and the subsequent formation of an amorphous geopolymeric network. However, the magnitude of this shift remains less pronounced than that typically reported for conventional metakaolin-based geopolymers (generally in the range of 950–990 cm^{-1}), [47, 48] suggesting a limited degree of structural reorganization in the present system. The main band centered at ~1000–1010 cm^{-1}, attributed to asymmetric stretching vibration of Si–O–T bonds, represents a characteristic fingerprint of geopolymer gel formation [12, 19, 48]. Its relatively broad shape and moderate intensity further indicate the coexistence of a partially disordered amorphous phase with residual crystalline components. The limited shift and spectral features observed here can be attributed to the low availability of reactive aluminum, resulting in a relatively high Si/Al ratio compared to typical geopolymeric systems (Si/Al ≈ 1–3) [35, 35, 49, 50]. This compositional constraint restricts the formation of a highly cross-linked aluminosilicate network. As a consequence, the geopolymeric gel formed is likely dominated by Si-rich structures, such as K–A–S–H-type gels, with possible involvement of Fe-bearing species due to the high Fe content of the precursor [32, 36, 51]. The reduced incorporation of Al into the framework limits the polymerization degree and network connectivity, thereby affecting the structural integrity of the material [50]. The persistence of crystalline phases together with the moderate shift of the main band indicates incomplete geopolymerization, which can be attributed to the low reactivity of Fe-rich phases and the unfavorable Si/Al ratio. These structural limitations are consistent with the relatively low mechanical performance observed, highlighting the critical role of precursor composition in controlling gel formation and network densification. Finally, the bands located at approximately 1640 cm^{-1} and 3430 cm^{-1} correspond to the bending and stretching vibrations of molecular water (H–O–H) and hydroxyl (–OH) groups, respectively, indicating the presence of physically bound water within the geopolymeric matrix [17, 31, 43].

Mineralogical characterization (XRD) of geopolymers

X-ray diffraction patterns of the synthesized geopolymers reveal clear and systematic mineralogical variations that strongly depend on the MK/TSFr ratio, highlighting the influence of precursor composition on reactivity and geopolymerization (Figure 8). The evolution of the diffraction features is consistent with trends reported in other studies of multi-precursor geopolymers, where the extent of amorphization and crystalline phase dissolution govern mechanical performance and structural development [52].

The GP:D0.12.T21 sample (100% MK) exhibits a pronounced amorphous hump between 18° and 25° (2θ), characteristic of substantial geopolymeric gel formation. This halo, together with the suppression of the original crystalline

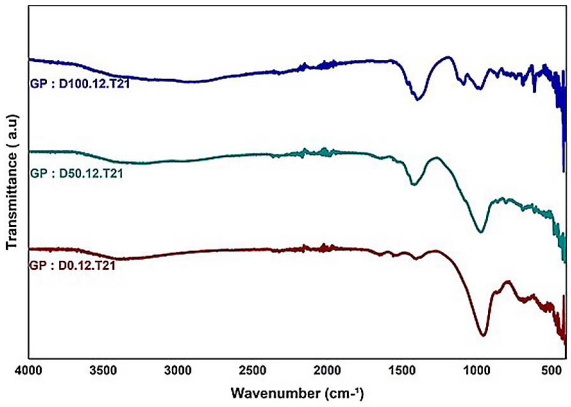

Figure 7. FTIR spectra of the synthesized geopolymers cured during 21 days (see Table 1)

reflections associated with metakaolin, reflects extensive dissolution of reactive aluminosilicate phases and the development of a highly disordered network. Similar behavior has been documented in metakaolin-based geopolymers, where the reduction of crystalline peaks and emergence of a broad amorphous background correlate with effective precursor dissolution and network condensation [53–55]. For the GP:D50.12.T21 sample (50% TSFr), the diffraction pattern shows a further reduction in the intensity of crystalline reflections compared to the raw materials and a moderate broadening of the amorphous hump. This suggests a synergistic interaction between MK and TSFr, facilitating partial dissolution of both precursors and contributing to the formation of a hybrid geopolymeric matrix. Such interactions have been observed in geopolymer systems incorporating fly ash or other mineral additives,

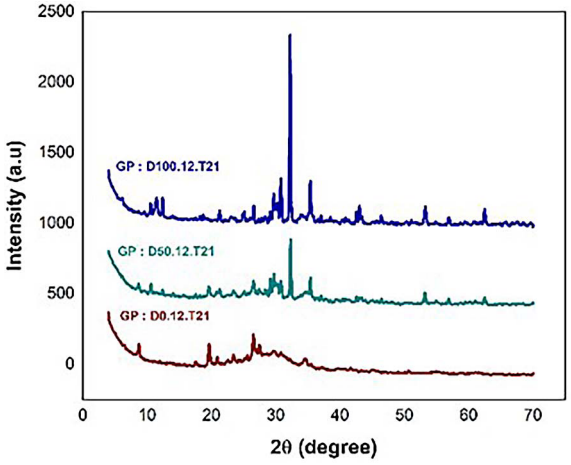

Figure 8. XRD patterns of the synthesized geopolymers cured during 21 days (see Table 1)

where balanced dissolution kinetics enhance network formation and densification [17]. In contrast, the GP:D100.12.T21 sample (100% TSFr) exhibits limited mineralogical evolution after alkaline activation. The diffraction pattern remains dominated by sharp crystalline peaks with only a weak and poorly developed amorphous halo. Peaks corresponding to iron-rich phases, particularly magnetite ($Fe^{2+}Fe_2^{3+}O_4$), persist and even intensify, indicating their low reactivity under the present alkaline conditions (Figure 8). The dominance of such inert phases, coupled with the low availability of reactive aluminum, hinders the formation of a continuous three-dimensional aluminosilicate gel network. This observation aligns with literature reporting that tailings-rich geopolymers often show reduced amorphous content and poorer mechanical performance due to insufficient dissolution of reactive components [56].

The comparison with raw precursor patterns confirms that the extent of amorphization decreases markedly with increasing TSFr content. This trend emphasizes that pure TSFr lacks sufficient reactive phases to develop a dense geopolymeric gel, in contrast to MK-dominated systems. Previous work has shown that successful geopolymerization generally requires a Si/Al balance and sufficient dissolution of aluminosilicate sources to enable polymerization and network formation [56].

Overall, the XRD results demonstrate that the degree of amorphization and phase transformation is controlled by the composition of the precursors, corroborating the known importance of precursor reactivity and Si/Al balance on geopolymer structure and properties [47, 57, 58].

Optical and SEM analysis of geopolymers

Observations of polished thin-sections under polarized-light optical microscopy confirmed the presence of amorphous material dispersed in the matrix and concentrated in ~500–1000 µm-diameter bubles (Figure 9), indicating that geopolymerization occurred. However, this reaction was not complete, as most TSFr-forming minerals (including magnetite, chalcopyrite, carbonates, quartz, phyllosilicates, K-feldspar, and iron hydroxides) remained largely unreacted. EDS-SEM analysis further revealed the persistence of potassium feldspar and iron hydroxides, highlighting the heterogeneous reactivity of the precursor phases. Microstructural of GP:D100.12.T21 shows that matrix homogeneity and precursor reactivity

strongly influence mechanical performance (Figure 10). White efflorescence deposits observed on the geopolymer cylinder surface (Figure 2: GP : D100.12.T21) indicate the presence of residual alkalis (K^+, Na^+) not incorporated into the geopolymeric network, consistent with FTIR observations showing weak geopolymerization bands in aluminum-deficient samples [8, 19, 50].

The geopolymer matrix exhibits microcracks and voids caused by water evaporation during curing, which reduce compactness and increase porosity. XRD analysis confirms that these regions correspond to persistent crystalline phases – particularly iron oxides such as magnetite and hematite – rather than the broad amorphous hump characteristic of fully polymerized geopolymer gel. EDS-SEM elemental mapping shows heterogeneous elemental distribution, with localized enrichment in Ca and Fe corresponding to non-reactive phases identified by XRD and FTIR (Figure 10). This incomplete reaction, coupled with the low availability of reactive aluminum, results in a predominantly Si-rich geopolymeric gel, possibly containing Fe-associated environments, rather than a well-developed N–A–S–H network, explaining the relatively low compressive strength observed (see next section).

Overall, the integration of optical petrographic microscopy, EDS-SEM, FTIR, and XRD demonstrates that the extent of geopolymerization is strongly controlled by precursor composition, Si/Al ratio, and phase reactivity. Our results emphasize the critical role of reactive aluminosilicates and phase distribution in achieving dense, mechanically robust geopolymers, as evidenced previously [19, 54, 59, 60].

It should be noted that the present characterization techniques provide indirect evidence of Fe participation in the geopolymerization process. Advanced techniques such as Mössbauer spectroscopy, XPS, solid-state NMR, or TEM would be required to confirm the exact coordination environment of Fe within the geopolymeric structure. Therefore, Fe incorporation is discussed here as a probable mechanism rather than a definitive atomic-scale assignment.

Compressive strength evolution of geopolymers

The compressive strength evolution of the synthesized geopolymers was systematically investigated after 7, 14, and 21 days of curing at 60 °C (Figure 11). For each formulation and curing age, the reported values correspond to the mean compressive strength obtained from three independent measurements, while the error bars represent the associated standard deviations, reflecting the reproducibility and experimental variability of the mechanical testing.

The GP:D0.12 formulation (100% metakaolin) exhibited a continuous increase in compressive strength with curing time, increasing from 7.0 MPa after 7 days to 8.5 MPa after 21 days, with an intermediate value of approximately 7.3

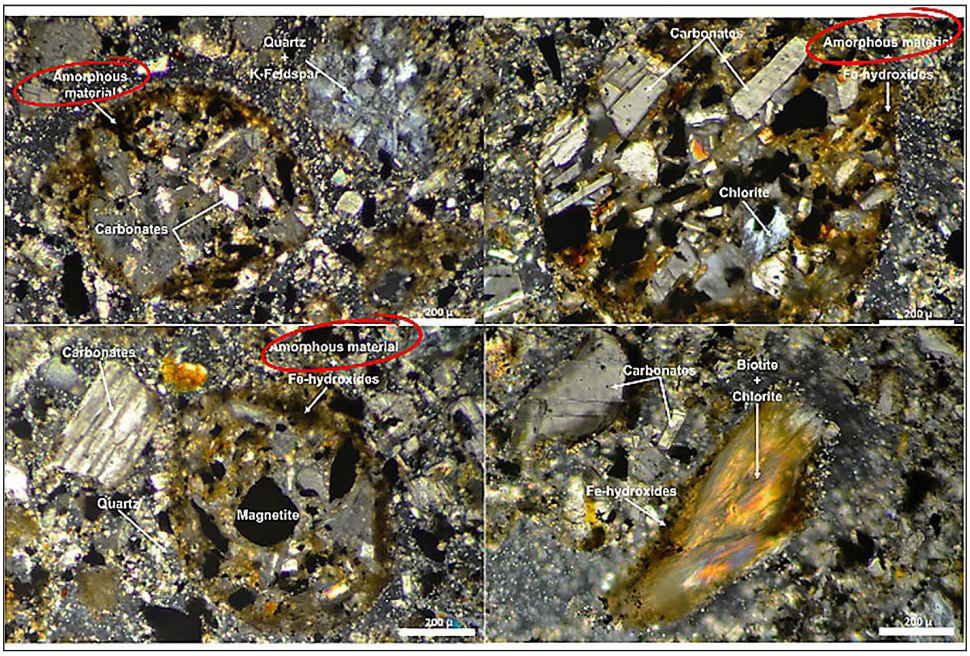

Figure 9. Transmitted-light optical microscopy petrographic thin-section images of geopolymer GP: D100.12.T21

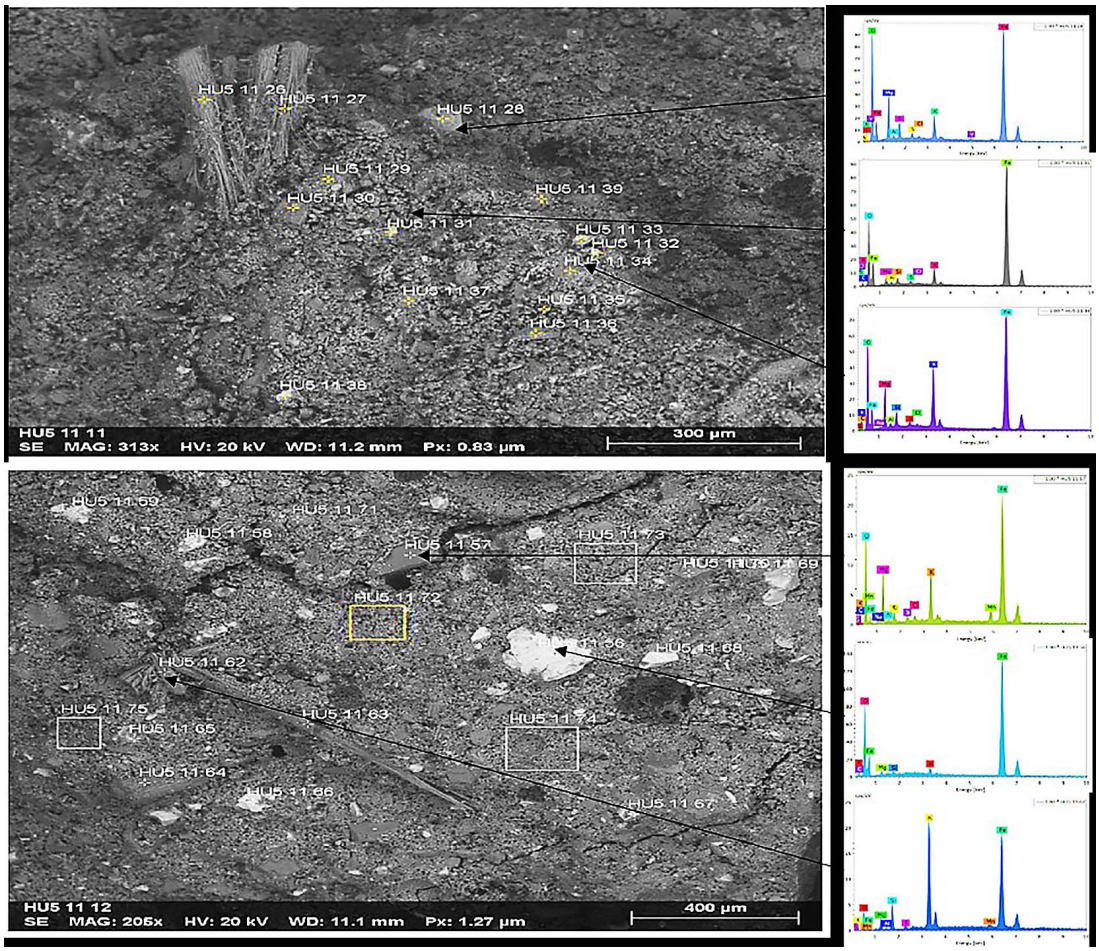

Figure 10. Rough surface SEM images and in-situ EDS-SEM chemical analyses of geopolymer GP: D100.12.T21

MPa after 14 days (Figure 11). This progressive strength development is attributed to the high reactivity of metakaolin, which provides a highly available aluminosilicate source promoting geopolymer network formation and progressive matrix densification. The broad amorphous halo observed in XRD patterns indicates the development of disordered aluminosilicate reaction products, while FTIR spectra reveal structural rearrangements within the aluminosilicate framework through the evolution of T–O–Si/Al vibrations, supporting the formation of geopolymeric reaction products [18, 61].

The GP:D50.12 formulation (50% TSFr and 50% metakaolin) showed a significant improvement in compressive strength with curing time, increasing from 4.8 MPa after 7 days to 8.0 MPa after 21 days. This behavior highlights the beneficial effect of combining iron-rich copper tailings with a reactive aluminosilicate precursor. The reduction in crystalline peak intensities observed in XRD patterns compared with the initial raw materials suggests partial dissolution and transformation of the precursor phases during alkaline activation. The presence of metakaolin enhances the availability of reactive Al species, favoring the development of an interconnected geopolymeric matrix. These structural evolutions are consistent with the improved mechanical performance, suggesting that the progressive development of the geopolymeric matrix and the possible contribution of Fe-bearing phases may influence the final properties of the material [58, 59].

In contrast, the GP:D100.12 formulation (100% TSFr) exhibited a more limited strength evolution, increasing from 6.0 MPa after 7 days to 7.0 MPa after 21 days, with an intermediate value of approximately 6.5 MPa after 14 days. The lower mechanical development compared with metakaolin-containing formulations can be related to the mineralogical characteristics of TSFr, particularly the limited availability of reactive aluminum species and the predominance of less reactive Fe-bearing crystalline phases. XRD patterns reveal the persistence of iron oxide-related reflections, while FTIR spectra show weaker

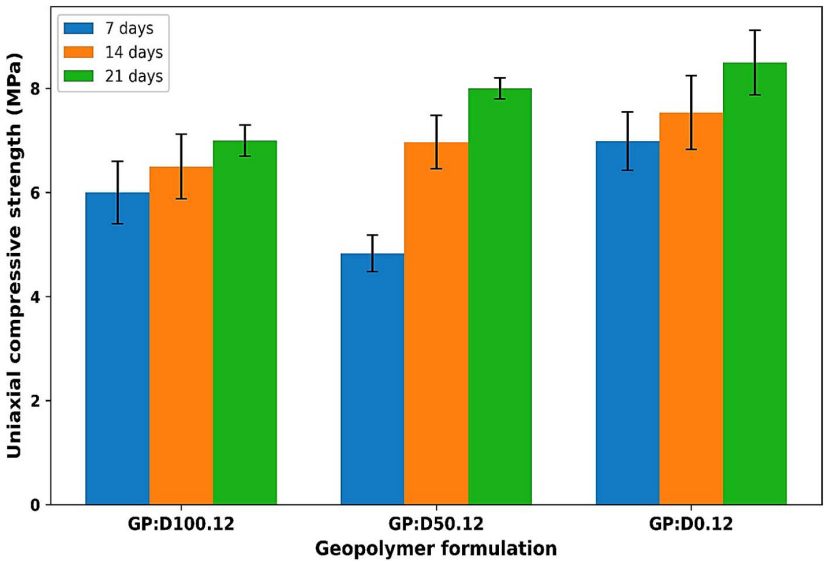

Figure 11. Uniaxial compressive strength evolution of synthesized geopolymers at different curing ages
Data are presented as mean ± standard deviation from three independent measurements (n = 3)

modifications associated with geopolymeric structural development, suggesting a lower extent of aluminosilicate network formation. SEM observations further support this interpretation by revealing a heterogeneous microstructure with local cavities and microcracks, which may limit matrix densification and mechanical performance [13, 37, 57, 62, 63].

The compressive strength results showed low variability among triplicate measurements, with standard deviations ranging from 0.20 to 0.71 MPa, corresponding approximately to 2.5–10% of the average strength values. This limited dispersion confirms the good repeatability of the mechanical testing procedure and supports the reliability of the observed strength evolution. The remaining variability can be attributed to the heterogeneous nature of mining tailings-based geopolymers and local differences in microstructural development during curing.

Overall, the results demonstrate that the mechanical performance of TSFr-based geopolymers is strongly controlled by the balance between waste incorporation and reactive aluminosilicate availability. The GP:D50.12 formulation represents an optimal compromise between mechanical performance and sustainable waste valorization, demonstrating the feasibility of incorporating iron-rich copper mine tailings into geopolymeric materials while maintaining competitive compressive strength.

Potential contaminant stabilization mechanisms

Environmental performance of geopolymer binders formulated from mining residues is a major issue. Contaminant potential stabilization relies on their conversion into precipitated phases of low solubility (hydroxides, carbonates, silicates, or) within the newly formed solid matrix [64] (Figure 12). This process is governed by three complementary mechanisms: chemical fixation, surface adsorption onto hydration products, and physical encapsulation, the latter being strictly dependent on the density and porous microstructure of the hardened paste [65,66]. In geopolymer matrices, immobilization occurs within a three-dimensional aluminosilicate network [67]. The primary mechanism involves the incorporation of metal ions into the structure to compensate for the negative charge of AlO_4^- tetrahedra (Figure 12). According to [45] this process takes place in three steps: integration of ions into the network, structural bonding for charge balance, and finally physical encapsulation of metallic precipitates [68]. This synergy is favored by the high alkalinity of the medium and the nanostructural organization of the geopolymer gel [69].

However, the predominance of one mechanism over another remains a subject of scientific debate. On one hand, many authors argue that physical encapsulation is the determining factor in stabilization efficiency. In dense, low-permeability matrices, reduced pore connectivity drastically limits contaminant transport [70, 71]. In

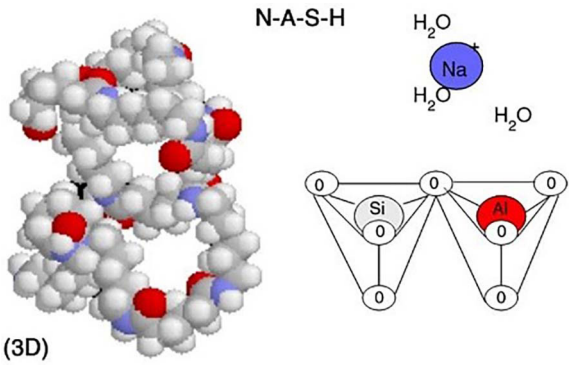

Figure 12. The three-dimensional structure of a N-A-S-H gel [71]

such systems, optimized dissolution of aluminum and silicon promotes polycondensation reactions, leading to a more compact structure. For example, the formation of highly insoluble lead silicates (Pb_3SiO_5), identified by XRD, suggests that Pb potential stabilization is mainly governed by encapsulation of precipitated phases. On the other hand, studies by [45] highlight the predominance of chemical potential stabilization, showing that elements such as arsenic preferentially associate with iron-rich amorphous phases within the matrix, suggesting chemical bonding rather than simple physical encapsulation [57]. Similarly, [61] indicated that in kaolin-zeolite systems, metal cations function as charge-balancing species within the geopolymeric network, with no significant alteration of the material's crystallinity.

However, the actual potential stabilization efficiency and environmental stability of the developed geopolymer materials were not experimentally evaluated in this study. Further investigations using standardized leaching procedures, such as TCLP, EN 12457, or SPLP tests, are required to quantitatively assess the retention of potentially hazardous elements.

CONCLUSIONS

This study provides new insights into the geopolymerization potential of iron-rich copper mine tailings from the Guelb Moghrein IOCG-type deposit (Mauritania), demonstrating their transformation from a mining waste into a functional geopolymeric material. The results highlight that the valorization of such complex Fe-bearing tailings requires a careful balance between waste incorporation and reactive aluminosilicate availability to achieve efficient geopolymer network development.

The combined mineralogical, spectroscopic, microstructural, and mechanical investigations confirmed that alkaline activation induced significant modifications of the original tailings structure and promoted the formation of geopolymeric reaction products. The incorporation of metakaolin enhanced the availability of reactive Si and Al species, facilitating the development of a more continuous and mechanically efficient aluminosilicate matrix. The evolution of Fe-bearing phases during activation suggests their involvement in the geopolymerization environment; however, their exact structural contribution at the atomic scale remains to be confirmed by advanced characterization techniques.

The mechanical performance demonstrated a clear curing-time dependence, with progressive strength development for all formulations. Among the investigated systems, the GP:D50.12 formulation achieved the most favorable balance, reaching approximately 8 MPa after 21 days while incorporating 50% mining tailings. This result highlights the possibility of achieving high waste substitution without compromising mechanical performance, representing a significant step toward sustainable geopolymeric construction materials based on mining residues.

The statistical analysis of compressive strength data, with low standard deviations (0.20–0.71 MPa), confirmed the reproducibility of the experimental approach and strengthened the reliability of the observed mechanical trends. Although the full replacement of metakaolin by TSFr resulted in a less developed geopolymeric network due to limited reactive aluminosilicate availability, the obtained results demonstrate the intrinsic potential of iron-rich copper tailings as a secondary raw material for geopolymer production.

Overall, this work advances the understanding of geopolymerization of Fe-rich mining residues by establishing a direct relationship between precursor composition, structural evolution, and mechanical behavior. It provides a sustainable pathway for the valorization of Guelb Moghrein copper tailings and opens new perspectives for the development of low-carbon construction materials from complex mining wastes.

Acknowledgements

Technical and research staff of the University of Granada are greatly appreciated for facilitating and helping in sample preparation, data adquisition and interpretation: Prof. Francisco Martín Peinado (Soils Lab., Dept. Edaphology and Agricultural Chemistry, Fac. Sciences); Prof. Fernando Nieto García, Prof. Giuseppe V. Cultrone and Eva María Marín Martín (XRD Lab., Dept. Mineralogy and Petrology), Prof. Fernando Gervilla Linares (Optical Microscopy Lab., Dept. Mineralogy and Petrology); Prof. Antonio Jabaloy Sánchez and Ángel Perandrés Villegas (Optical Microscopy and Thin-Sections Labs., Dept. Geodynamics); Dr. Isabel Sánchez Almazo (ESEM Unit), Dr. Laura Crespo-López López (FTIR Unit), Olga Cazalla Vázquez (ICP-MS Unit), and Carlos Gutiérrez Ariza (Nanoindentation Unit) of the Scientific Instrumentation Center (UGR).

REFERENCES

1. Alsalman, A., Assi, L. N., Kareem, R. S., Carter, K., and Ziehl, P., (2021). Évaluation de la consommation énergétique et des émissions de CO_2 du béton activé aux alcalis et du béton de ciment Portland ordinaire : une analyse comparative de différentes qualités de béton, *Cleaner Environmental Systems, 3*, 100047.
2. Davidovits, J., (2017). Geopolymers: Ceramic-like inorganic polymers, *Journal Of Ceramic Science And Technology, 8*, 335–350.
3. Sracek, O., Kříbek, B., Mihaljevič, M., Majer, V., Veselovský, F., Vencelides, Z., and Nyambe, I., (2012). Mining-related contamination of surface water and sediments of the Kafue River drainage system in the Copperbelt district, Zambia: An example of a high neutralization capacity system, *Journal Of Geochemical Exploration, 112*, 174–188.
4. Dold, B., (2017). Acid rock drainage prediction: A critical review, *Journal Of Geochemical Exploration*, *172*, 120–132.
5. Valente, T., (2023). Editorial for Special Issue Pollutants in Acid Mine Drainage, *Minerals, 13*(7), 931.
6. Singer, P. C., Stumm, W. (1970). Acid mine drainage the rate-determining step. *Science, 167*, 1121–1123. – References – Scientific Research Publishing, doi.org/10.1126/science.167.3921.1121
7. Palma, G., Bolaños, H., Huamani, R., Clements, C., and Hedayat, A., (2024). Optimization of geopolymers for sustainable management of mine tailings: impact on mechanical, microstructural, and toxicological properties, *Minerals, 14*(10), 997.
8. Al-Attar, T., Al-Shathr, B., and Hasan, Z., (2015). Optimization of Geopolymer Concrete Based on Local Iraqi Metakaolin, *The 2nd International Conference of Buildings, Construction and Environmental Engineering (BCEE2-2015).*
9. Abdila, S. R., Abdullah, M. M. A. B., Ahmad, R., Burduhos Nergis, D. D., Rahim, S. Z. A., Omar, M. F., Sandu, A. V., Vizureanu, P., and Syafwandi, (2022). Potential of soil stabilization using ground granulated blast furnace slag (GGBFS) and fly ash via geopolymerization method: A review, *Materials, 15*(1), 375.
10. Autef, A., Joussein, E., Gasgnier, G., and Rossignol, S., (2012). Role of the silica source on the geopolymerization rate, *Journal Of Non-Crystalline Solids, 358*(21), 2886–2893.
11. Singh, J. and Singh, S. P., (2019). Geopolymerization of solid waste of non-ferrous metallurgy – A review, *Journal Of Environmental Management, 251*, 109571
12. Cunha, J., Ferreira, I., Campos, L., Galery, R., and Mazzinghy, D., (2025). Geopolymer as an alternative stabilizer of waste and tailings from iron mining, *Tecnologia Em Metalurgia, Materiais E Mineração, 22*, e3201.
13. Feng, Z., Zhang, Z., Li, W., Hao, G., Xia, X., Li, P., and Zhu, K., (2025). Recent advances in tailings waste as geopolymers for construction: Current challenges and prospects, *Minerals Engineering, 230*, 109439.
14. Venkatesan, G., Alengaram, U. J., Ibrahim, S., and Ibrahim, M. S. I., (2024). Effect of Fly Ash characteristics, sodium-based alkaline activators, and process variables on the compressive strength of siliceous Fly Ash geopolymers with microstructural properties: A comprehensive review, *Construction And Building Materials, 437*, 136808.
15. Kazemian, F. and Hassani, A., (2024). Exploring mechanical and fracture properties in geopolymer concrete with ternary precursor waste materials through laboratory investigations and statistical analysis, *Journal Of Building Engineering, 95*, 110294.
16. Vogt, O., Ukrainczyk, N., Ballschmiede, C., and Koenders, E., (2019). Reactivity and Microstructure of Metakaolin Based Geopolymers: Effect of Fly Ash and Liquid/Solid Contents, *Materials, 12*(21).
17. Wang, H., Li, H., and Yan, F., (2005). Synthesis and mechanical properties of metakaolinite-based geopolymer, *Colloids And Surfaces A: Physicochemical And Engineering Aspects, 268*(1), 1–6.
18. Bai, C., Zheng, K., Sun, F., Wang, X., Zhang, L., Zheng, T., Colombo, P., and Wang, B., (2024). A review on metakaolin-based porous geopolymers, *Applied Clay Science, 258*, 107490.

19. Martyn, J., Strickland, C. (2004). Stratigraphy, structure and mineralisation of the Akjoujt area, Mauritania, *Journal of African Earth Sciences, 38*, 489–503.
20. Jiménez Borrego, R., Martínez Poyatos, D., Azor, A., Accotto, C., Jabaloy-Sánchez, A., González Lodeiro, F.,..., Ould Ely Lekouyrie, A., (2026). Persistent amazonian and West African detrital zircon signature in the northern Mauritanide Belt, *Gondwana Reseach, 149*, 1–16.
21. Kolb, J., Meyer, F., Prantl, S., Sindern, S., Sakellaris, G. A., Vennemann, T., and Böttcher, M., (2010). *Characteristics of Hydrothermal Fluids Forming the Guelb Moghrein Fe Oxide-Cu-Au-Co Deposit, Mauritania: Ore Mineral Chemistry, Fluid Inclusions and Isotope Geochemistry.,* Porter, T.M. (Ed.), 2010 - Hydrothermal Iron Oxide Copper-Gold And Related Deposits: A Global Perspective, Vol. 4, PGC Publishing, Adelaide. 298p.
22. Pouclet, A., Guillot, P.-L., and Ba Gatta, A., (1987). Nouvelles données lithostructurales, pétrographiques, minéralogiques et géochimiques sur le gisement de cuivre d'Akjoujt et son environment géologique (République Islamique de Mauritanie), *Journal Of African Earth Sciences, 6*(1), 29–43.
23. Kolb, J., Sakellaris, G. A., and Meyer, F. M., (2006). Controls on hydrothermal Fe oxide–Cu–Au–Co mineralization at the Guelb Moghrein deposit, Akjoujt area, Mauritania, *Mineralium Deposita, 41*(1), 68–81.
24. Bureau, M., Survey, G., and Department, I., (2015). Minerals Yearbook: Area Reports: International Review 2012 Africa and the Middle East, *Government Printing Office, 426.*
25. Fernette, G. (2012). *Dépôts d'oxyde de fer cuivre-or en Mauritanie (Livrable 79). Second Projet de Renforcement Institutionnel du Secteur Minier de la République Islamique de Mauritanie (PRISM-II),* Phase V. U.S. Geological Survey.
26. Barreto, I. A. R. and da Costa, M. L., (2022). Synthesis of geopolymer with KOH by two kaolinitic clays from the Amazon: Influence of different synthesis parameters on the compressive strength, *Materials Chemistry And Physics, 287*, 126330.
27. Xiong, L., Wan, Z., Zhang, Y., Wang, F., Wang, J., and Kang, Y., (2019). Fly ash particle size effect on pore structure and strength of fly ash foamed geopolymer, *Advances In Polymer Technology*, (1), 1098027.
28. Nath, S. and Kumar, S., (2019). Role of particle fineness on engineering properties and microstructure of fly ash derived geopolymer, *Construction And Building Materials, 233*.
29. Abdullah, M. M. A. B., Kamarudin, H., Binhussain, M., Nizar, K., Yahya, Z., and Razak, R., (2011). The effect of curing temperature on physical and chemical properties of geopolymers, *2011 International Conference On Physics Science And Technology*, Elsevier Science, Amsterdam, 286–291.
30. Temuujin, J., Williams, R.P. et Van Riessen, A.V. (2009). Effet de l'activation mécanique des cendres volantes sur les propriétés du géopolymère durci à température ambiante. *Journal of materials processing technology*, *209*(12–13), 5276–5280.
31. Al-Shathr, B. S., Al-Attar, T. S., and Hasan, Z. A., (2016). Effect of curing system on metakaolin based geopolymer concrete, *Engineering Sciences.*
32. Alaba, P., Sani, Y. M., and Daud, W., (2015). Kaolinite properties and advances for solid acid and basic catalyst synthesis, *RSC Advances, 5*, 101127–101147.
33. Deligöz, H., Baykal, A., Tanrıverdi, E. E., Durmus, Z., and Toprak, M. S., (2012). Synthèse, propriétés structurales et électriques de nanoparticules de $Mn_{0,2}$ $Co_{0,8}$ Fe_2O_4 stabilisées par du triéthylène glycol (TREG), *Materials Research Bulletin, 47*(3), 537–543.
34. Andrade, A. L., Souza, D. M., Pereira, M. C., Fabris, J. D., and Domingues, R. Z., (2009). Synthesis and characterization of magnetic nanoparticles coated with silica through a sol-gel approach, *Cerâmica, 55*, 420–424.
35. Cui, H., Ren, W., Lin, P., and Liu, Y., (2013). Structure control synthesis of iron oxide polymorph nanoparticles through an epoxide precipitation route, *Journal Of Experimental Nanoscience, 8*(7–8), 869–875.
36. Essaidi, N., Samet, B., Baklouti, S., and Rossignol, S., (2014).The role of hematite in aluminosilicate gels based on metakaolin, *Ceramics Silikati, 58*(1), 1–11.
37. Ngintedem, D., Siéwé, J., Tchakoute Kouamo, H., and Rüscher, C., (2024). Microstructure and compressive strength of geopolymer materials based on metakaolin with hematite and magnetite gels as additives, *Sustainable Chemical Engineering, 5*, 332–351.
38. Zibouche, F., (2013). Géopolymérisation d'aluminosilicates. Influence des rapports Silice/Alumine, *Journal Of Materials, Processes And Environment, 1*(2), 147–156.
39. Weng, L. and Sagoe-Crentsil, K., (2007). Dissolution processes, hydrolysis and condensation reactions during geopolymer synthesis: Part I—Low Si/Al ratio systems, *Journal of Materials Science, 42*(9), 2997–3006.
40. Yong, H., Kamarudin, H., Abdullah, M. M. A. B., Binhussain, M., Musa, L., Nizar, K., Ruzaidi, C., and Ming, L., (2012). Study on solids-to-liquid and alkaline activator ratios on kaolin-based geopolymers, *Construction And Building Materials, 35*.

41. Silva, P. D., Sagoe-Crenstil, K., and Sirivivatnanon, V., (2007). Cinétique de la géopolymérisation : rôle de Al_2O_3 et de SiO_2, *Cement And Concrete Research, 37*(4), 512–518.
42. Gougazeh, M. and Buhl, J.-C., (2010). Geochemical and mineralogical characterization of the Jabal Al-Harad kaolin deposit, southern Jordan, for its possible utilization, *Clay Minerals, 45*.
43. Aragaw, T. A., (2020). The effect of mechanical treatment and calcination temperature of Ethiopian kaolin on amorphous metakaolin product, *Conference: International Conference on Advances of Science and Technology*, 308671.
44. Aragaw, T. A. and Ayalew, A., (2019). Removal of water hardness using zeolite synthesized from Ethiopian kaolin by hydrothermal method, *Water Practice & Technology, 14*: 145–159.
45. Nadeif, A., Taha, Y., Bouzahzah, H., Hakkou, R., and Benzaazoua, M., (2019). Desulfurization of the old tailings at the Au-Ag-Cu Tiouit Mine (Anti-Atlas Morocco), *Minerals, 9*(7), 401.
46. Chopard, A., (2016). *Évaluation environnementale et géométallurgique de minerais sulfurés polymétalliques, basée sur une approche minéralogique pluridisciplinaire*, Theses, Université de Lorraine.
47. Lengke, M. F. and Tempel, R. N., (2005). Geochemical modeling of arsenic sulfide oxidation kinetics in a mining environment, *Geochimica Et Cosmochimica Acta, 69*(2), 341–356.
48. Pisciella, P. and Pelino, M., (2005). FTIR spectroscopy investigation of the crystallisation process in an iron rich glass, *Journal Of The European Ceramic Society, 25*(11), 1855–1861.
49. Nikolov, A. and Karamanov, A., (2022). Thermal properties of geopolymer based on fayalite waste from copper production and metakaolin, *Materials, 15*(7), 2666.
50. Zaharaki, D., Komnitsas, K., and Perdikatsis, V., (2010). Use of analytical techniques for identification of inorganic polymer gel composition, *Journal Of Materials Science, 45*, 2715–2724.
51. Essaidi, N., Samet, B., Baklouti, S., and Rossignol, S., (2013). Effect of calcination temperature of tunisian clays on the properties of geopolymers, *Ceramics - Silikaty, 57*.
52. Riahi, M., (2017). Properties of metakaolin based geopolymer incorporating calcium carbonate, *Advanced Powder Technology.*
53. Maged, A., El-Fattah, H. A., Kamel, R. M., Kharbish, S., and Elgarahy, A. M., (2023). A comprehensive review on sustainable clay-based geopolymers for wastewater treatment: circular economy and future outlook, *Environmental Monitoring And Assessment, 195*(6), 693.
54. Ali Siyal, A., Mohamed, R. M. S. R., Shamsuddin, R., and Baharudin Ridzuan, M., (2024). A comprehensive review of synthesis kinetics and formation mechanism of geopolymers, *RSC Advances, 14*(1), 446–462.
55. Lemougna, P. N., MacKenzie, K. J. D., Jameson, G. N. L., Rahier, H., and Chinje Melo, U. F., (2013). The role of iron in the formation of inorganic polymers (geopolymers) from volcanic ash: a 57Fe Mössbauer spectroscopy study, *Journal Of Materials Science, 48*(15), 5280–5286.
56. Bundy, W. M. and Murray, H. H., (1973). The effect of aluminum on the surface properties of kaolinite, *Clays And Clay Minerals, 21*(5), 295–302.
57. Park, S. and Pour-Ghaz, M., (2018). What is the role of water in the geopolymerization of metakaolin?, *Construction And Building Materials, 182*, 360–370.
58. Xie, T., Ozbakkaloglu, T. (2015). Comportement du béton géopolymère à base de cendres volantes et de cendres de fond à faible teneur en calcium durci à température ambiante. *Ceramics International*, *41*(4), 5945–5958.
59. Cong, P. and Cheng, Y., (2021). Advances in geopolymer materials: A comprehensive review, *Journal Of Traffic And Transportation Engineering, 8*(3), 283–314.
60. Ngintedem, D., Lampe, M., Tchakoute Kouamo, H., and Rüscher, C., (2022). Effects of iron minerals on the compressive strengths and microstructural properties of metakaolin-based geopolymer materials, *Gels, 8*, 525.
61. Vu, T.H, Gowripalan, N. (2018). Mécanismes d'immobilisation des métaux lourds à l'aide de techniques de géopolymérisation – une revue. *Journal of Advanced Concrete Technology, 16*(3), 124–135.
62. Girardin, P., Guichardon, P., Millard, A. (2019). Proposition en réponse à l'appel à projet ANCRE_SdBE_2020: Le conditionnement des déchets nucléaires en matrice cimentaire–Développement de la modélisation pour l'extrapolation des essais de l'échelle laboratoire vers l'échelle industrielle.
63. Spence, R. D. and Shi, C., (2004). Stabilization and solidification of hazardous, radioactive, and mixed wastes, *Stabilization and Solidification of Hazardous, Radioactive, and Mixed Wastes, 379,* 1.
64. Granizo, N., Palomo, A., Fernandez-Jiménez, A., (2014). Effect of temperature and alkaline concentration on metakaolin leaching kinetics, *Ceramics International*, *40*(7), 8975–8985.
65. Zheng, L., Wang, W., and Shi, Y., (2010). The effects of alkaline dosage and Si/Al ratio on the immobilization of heavy metals in municipal solid waste incineration fly ash-based geopolymer, *Chemosphere, 79*(6), 665–671.
66. Vu, T. H., Gowripalan, N., (2018). Mechanisms of heavy metal immobilisation using geopolymerisation

techniques–a review, *Journal of Advanced Concrete Technology*, *16*(3), 124–135.

67. Palacios, M. and Palomo, A., (2004). Alkali-activated fly ash matrices for lead immobilisation: a comparison of different leaching tests, *Advances In Cement Research, 16*(4), 137–144.
68. Phair, J. W. and Van Deventer, J. S. J., (2001). Effect of silicate activator pH on the leaching and material characteristics of waste-based inorganic polymers, *Minerals Engineering, 14*(3), 289–304.
69. Fernández-Jiménez, A., MacPhee, D. E., Lachowski, E. E., Palomo, A., (2005). Immobilization of cesium in alkaline activated fly ash matrix, *Journal of nuclear materials*, *346*(2–3), 185–193.
70. El-Eswed, B. I., Yousef, R. I., Alshaaer, M., Hamadneh, I., Al-Gharabli, S. I., and Khalili, F., (2015). Stabilization/solidification of heavy metals in kaolin/zeolite based geopolymers, *International Journal Of Mineral Processing, 137*, 34–42.
71. Palomo, A., Krivenko, P., García-Lodeiro, I., Kavalerova, E., Maltseva, O., and Fernández-Jiménez, A., (2014). A review on alkaline activation: new analytical perspectives, *Materiales De Construcción, 64*(315), e022.